Experimental Realization of Linear-Optical Partial SWAP Gates

Antonín Černoch,[1] Jan Soubusta,[1] Lucie Bartůšková,[2] Miloslav Dušek,[2] and Jaromír Fiurášek[2]

[1]*Joint Laboratory of Optics of Palacký University and Institute of Physics of Academy of Sciences of the Czech Republic, 17. listopadu 50A, 779 07 Olomouc, Czech Republic*

[2]*Department of Optics, Palacký University, 17. listopadu 50, 772 00 Olomouc, Czech Republic*

(Received 29 November 2007; published 6 May 2008)

We present a linear-optical implementation of a class of two-qubit partial SWAP gates for polarization states of photons. Different gate operations, including the SWAP and entangling $\sqrt{\text{SWAP}}$, can be obtained by changing a classical control parameter, namely, the path difference in the interferometer. Reconstruction of output states, full quantum process tomography, and an evaluation of entanglement of formation prove very good performance of the gates.

DOI: 10.1103/PhysRevLett.100.180501 PACS numbers: 03.67.Lx, 42.50.−p

Quantum-information processing requires precise control and manipulation of the states of quantum systems. In particular, two-qubit entangling unitary gates lie at the heart of many protocols, and they are, together with single-qubit operations, sufficient for universal quantum computing [1]. The archetypal two-qubit controlled-NOT (CNOT) gate, or its equivalent, has been demonstrated for several physical systems, notably trapped ions [2], nuclear magnetic spins [3], and polarization states of single photons [4–12]. A specific feature of the linear-optical quantum gates for photonic qubits is that the required nonlinear coupling between two photons is achieved by using interference, auxiliary photons, single-photon detectors, and/or conditioning [13–16]. A universal quantum computer can be built with these resources despite the fact that the basic gates are only probabilistic and have some finite probability of failure [13,17].

In the experiments, correlated photon pairs generated by means of spontaneous parametric down-conversion are utilized. Consequently, the coincidence rate decreases rapidly with the number of photons limiting current experiments to six-photon coincidences [18]. Each nondestructive scalable CNOT gate requires at least two ancilla photons [6,7,13]. This makes it currently practically impossible to build more complex linear-optics logic circuits by concatenating several nondestructive CNOT gates. It is therefore highly desirable to seek other means of realizing various gates with available resources [19].

In this Letter, we report on experimental realization of a class of entangling partial SWAP gates for polarization states of photons. Besides quantum-information processing applications these gates can be employed to investigate decoherence in the process of quantum homogenization [20]. A simple modification of our setup also allows to implement partial symmetrization of polarization state of two photons, which can be used, together with auxiliary photons and passive linear optics, e.g., to emulate amplification of photon pairs with arbitrary gain [21].

The partial SWAP gate imposes a phase shift ϕ to singlet Bell state $|\Psi^-\rangle = \frac{1}{\sqrt{2}}(|H\rangle|V\rangle - |V\rangle|H\rangle)$ while it leaves unchanged the triplet Bell states $|\Psi^+\rangle = \frac{1}{\sqrt{2}} \times (|H\rangle|V\rangle + |V\rangle|H\rangle)$ and $|\Phi^\pm\rangle = \frac{1}{\sqrt{2}}(|H\rangle|H\rangle \pm |V\rangle|V\rangle)$. The unitary operation can be expressed as

$$U_\phi = \Pi_+ + e^{i\phi}\Pi_-, \tag{1}$$

where $\Pi_- = |\Psi^-\rangle\langle\Psi^-|$ and $\Pi_+ = I - \Pi_-$ are the projectors onto the antisymmetric and symmetric subspaces of two qubits, respectively, and I denotes the identity operator. $|H\rangle$ and $|V\rangle$ denote horizontal and vertical polarization state of a single photon. In this notation, the diagonal and antidiagonal linear polarization states read $|D\rangle = \frac{1}{\sqrt{2}} \times (|H\rangle + |V\rangle)$ and $|A\rangle = \frac{1}{\sqrt{2}}(|H\rangle - |V\rangle)$, and the right- and left-handed circular polarizations are given by $|R\rangle = \frac{1}{\sqrt{2}} \times (|H\rangle + i|V\rangle)$ and $|L\rangle = \frac{1}{\sqrt{2}}(|H\rangle - i|V\rangle)$.

The gates (1) are generally locally inequivalent to the CNOT or controlled-phase (CPHASE) gates demonstrated previously [4–10]. This means that the gate U_ϕ cannot be decomposed as a single CNOT gate accompanied by single-qubit operations at the input and output. In general, a sequence of up to three CNOT gates combined with single-qubit transformations is required [22], which would be extremely challenging to implement with present-day technology. Our approach bypasses this hurdle by combining single- and two-photon interference to directly realize the transformation (1). We utilize balanced Mach-Zehnder interferometer with two additional 50:50 beam splitters placed in each of its arms; see Fig. 1. The device operates in the coincidence basis [16]; i.e., the gate is successful only if we detect a single photon in each output port, similarly as in other implementations [8–10,12].

Let us describe the gate functioning in some detail. The photons impinge on the first beam splitter BS_1 where Hong-Ou-Mandel interference takes place [23]. BS_1 acts as a filter that distinguishes between symmetric and antisymmetric states of the photons. If the photons are in symmetric state, then they bunch and both end up in either the upper or the lower arm. In this case, the only way the photons are able to reach the proper output ports is to have

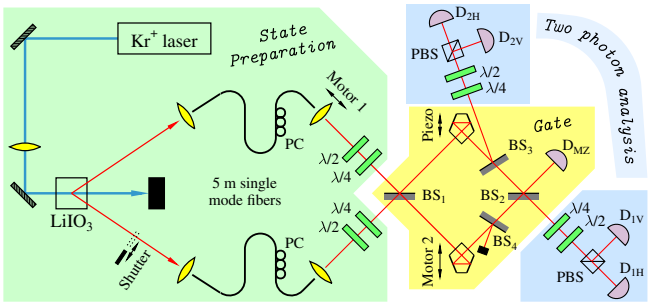

FIG. 1 (color online). Experimental setup: PC, fiber polarization controller; BS, nonpolarizing plate beam splitter; PBS, polarizing cube beam splitter; $\lambda/2$ and $\lambda/4$, wave plates; D, a set composed of cutoff filter, collimating lens, single-mode fiber, and avalanche photodiode.

them both travel through the upper arm; one photon is reflected from BS_3, and the other is transmitted through BS_3 and BS_2. On the other hand, if the photons are initially in the antisymmetric singlet state $|\Psi^-\rangle$, then each photon travels through one arm. By changing the optical path difference the singlet state can acquire arbitrary relative phase shift ϕ with respect to the triplet states. The conditionally applied transformation is given by Eq. (1), and the probability of success is equal to $\frac{1}{8}$. By additional attenuation of the signal in the lower arm the interferometer could operate also as a partial symmetrization device conditionally applying filter $\Pi_+ + \epsilon\Pi_-$ with $\epsilon < 1$ [21].

The experimental setup is schematically divided into three parts; see Fig. 1. The first part is the source of the time-correlated pairs of photons. The second part represents the gate, and the last part serves for two-photon polarization analysis. Pairs of photons are generated in the process of type I spontaneous parametric down-conversion in a nonlinear crystal of $LiIO_3$. The crystal is pumped by the cw Krypton-ion laser at 413 nm with power of 120 mW. The down-converted photons are coupled into two single-mode fibers and transferred to a second optical table. The two photons are released back to free space and the desired polarization state of each photon is set by means of half- and quarter-wave plates.

The second part of the setup represents the gate. As detailed above, it is formed by a standard Mach-Zehnder (MZ) interferometer with two additional balanced beam splitters in each arm. BS_3 splits out part of the beam for further processing, while BS_4 just balances the losses. Detector D_{MZ} monitors the interference fringes. This output is polarization independent so the signal from the detector D_{MZ} is used for active phase stabilization of the MZ interferometer.

The two-photon analysis is performed by coincidence polarization measurements between two blocks. Each block is composed of the quarter- and half-wave plate and a polarizing beam splitter (PBS), which splits the photon state into horizontal and vertical polarization components. Before detection the beams are filtered spectrally by cutoff filters at 780 nm, and geometrically by single-mode fibers to ensure perfect overlap of the spatial modes. The signals from avalanche photodiodes are processed by the four-input coincidence logic module.

Preliminary alignment of the setup is done in three steps. First, the proper function of the photon-pair source is verified. A separate fiber beam splitter is used to measure two-photon interference in Hong-Ou-Mandel–type interferometer (not shown in Fig. 1) [23]. Then the fiber beam splitter is replaced by two 5 m long fibers. Polarization controllers (PC) on the fibers serve to adjust horizontal linear polarizations at the output of the fibers. In the second step, the beam is blocked between beam splitters BS_3 and BS_2 and the overlap of the beams on the first beam splitter BS_1 is optimized. We scan the Hong-Ou-Mandel–type interference dip measuring coincidences between detectors D_{1H} and D_{2H} as a function of motor 1 position. In this configuration, the visibility is about 97%. Motor 1 position is placed to the minimum of the dip. As the last step we adjust the single-photon interference in the MZ interferometer. For this purpose, one input arm is blocked by the shutter in the source and BS_2 is realigned. The lengths of the interferometer arms are balanced by motorized translation of one pentagon prism (motor 2) to obtain the highest visibility of the interference fringes. Precise fringe phase scan is performed by piezodriven translation of the pentagon in the other arm and we typically observe visibility at about 98%.

In our experiment we performed full polarization analysis of the output two-photon state for various input product states. We measured two-photon coincidence counts between detectors D_{1H} and D_{2H}, D_{1V} and D_{2V}, D_{1H} and D_{2V}, and D_{1V} and D_{2H} for 9 (3×3) combinations of the measurement basis, i.e., projections onto H-V, D-A and R-L polarizations in the two output arms. The unequal detector efficiencies were compensated by proper rescaling of the measured coincidences [24]. The state analysis was made for 36 (6×6) combinations of the input polarization states $|H\rangle$, $|V\rangle$, $|D\rangle$, $|A\rangle$, $|R\rangle$, and $|L\rangle$. We measured the gate operation for nine values of the phase shift ϕ in the MZ interferometer, $\phi = k\pi/4$, $k = 0, \ldots, 8$. Each of these 2916 points was measured for 15 s. After each three measurement points the active stabilization procedure was performed as follows. The shutter blocked one arm in the source and with the help of detector D_{MZ} the zero phase position in the fringe pattern was updated. As a result, the interferometer was stable and the overall phase drift was negligible for a period of hours. There were only small oscillations $\lesssim 3\%$ of the period.

From the tomographically complete data we reconstructed the output two-qubit state corresponding to each input state. Standard maximum-likelihood (ML) estimation technique was employed [25,26]. As an example, Fig. 2 shows the reconstructed output density matrix for

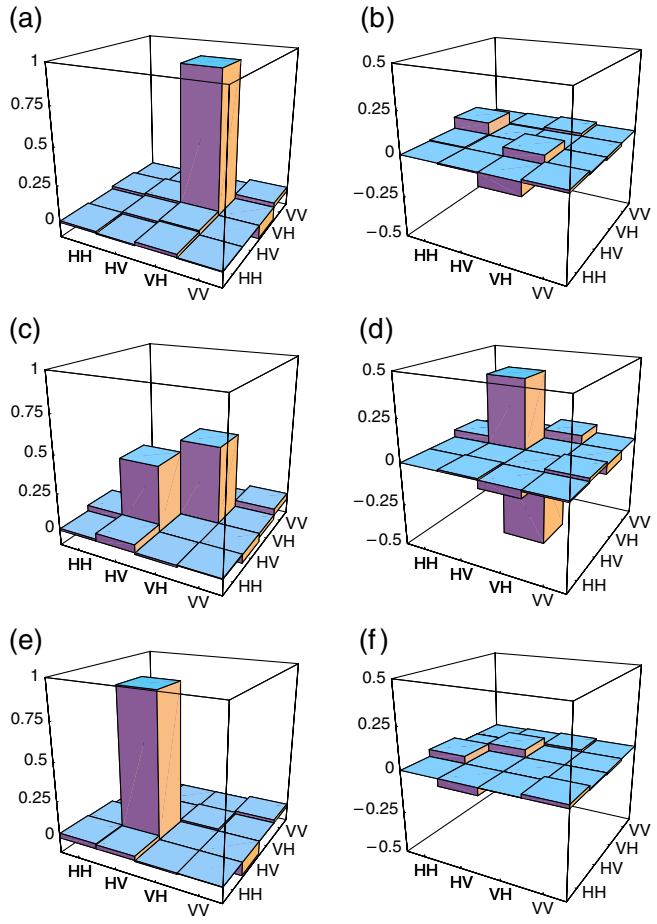

FIG. 2 (color online). Real (left column) and imaginary (right column) parts of the reconstructed output density matrix for input state $|V\rangle|H\rangle$ are shown for three different phase shifts $\phi = 0$ (a),(b), $\phi = \pi/2$ (c),(d), and $\phi = \pi$ (e),(f).

the input state $|V\rangle|H\rangle$ and three different values of the phase shift. For $\phi = 0$, the interferometer should realize identity operation, and the output state is indeed almost identical with the input pure state $|V\rangle|H\rangle$, with fidelity $F_0 = 0.947$. When we set $\phi = \pi/2$, the device realizes the square root of the SWAP operation ($\sqrt{\text{SWAP}}$). This gate is entangling and ideally should produce maximally entangled state $\frac{1}{\sqrt{2}}(|V\rangle|H\rangle - i|H\rangle|V\rangle)$. The creation of this state is clearly visible in Figs. 2(c) and 2(d) with coherence appearing in the imaginary part of the density matrix and its fidelity reads $F_{\pi/2} = 0.892$. Finally, for $\phi = \pi$ we get the output of the SWAP gate. Again, the result agrees very well with the expected outcome $|H\rangle|V\rangle$, and $F_\pi = 0.936$.

Table I contains the state fidelity F_{av} averaged over 36 output states corresponding to input product states $|j\rangle|k\rangle$, $j, k \in \{H, V, D, A, R, L\}$. The table also shows the minimum fidelity F_{min} among these 36 states. Another important characteristic of the state ρ is the purity, defined as $\mathcal{P} = \text{Tr}[\rho^2]$. The average and minimal purities of output states, which should ideally be pure with $\mathcal{P} = 1$, are also

TABLE I. Average and minimum fidelities and purities of the output states and the process fidelity for 9 different phase shifts ϕ.

ϕ	F_{av}	F_{min}	$\mathcal{P}_{\text{av}}$	$\mathcal{P}_{\text{min}}$	F_χ
0	0.960	0.930	0.957	0.917	0.946
$\pi/4$	0.942	0.892	0.938	0.863	0.928
$\pi/2$	0.924	0.876	0.895	0.804	0.906
$3\pi/4$	0.929	0.878	0.908	0.820	0.914
π	0.956	0.929	0.956	0.904	0.942
$5\pi/4$	0.943	0.882	0.939	0.848	0.930
$3\pi/2$	0.910	0.849	0.900	0.790	0.888
$7\pi/4$	0.941	0.875	0.923	0.831	0.923
2π	0.959	0.926	0.959	0.901	0.945

given in Table I. All these data confirm that the gate exhibits very good performance. The best results are achieved for the identity and SWAP operations. The most "difficult" operation turns out to be the $\sqrt{\text{SWAP}}$ ($\phi = \pi/2$ and $\phi = 3\pi/2$). But even in these cases the average state fidelity is above 90%.

The quantum gate can be fully characterized by a completely positive (CP) map. According to the Jamiolkowski-Choi isomorphism, the CP map can be represented by a positive semidefinite operator χ on the tensor product of input and output Hilbert spaces $\mathcal{H}_{\text{in}}$ and $\mathcal{H}_{\text{out}}$. In our case χ is thus a square matrix 16×16. The input state ρ_{in} transforms according to $\rho_{\text{out}} = \text{Tr}_{\text{in}}[\chi \rho_{\text{in}}^T \otimes I_{\text{out}}]$. Since our implementation is only probabilistic, we allow for general trace-decreasing map χ. Combinations of input states and corresponding measurement bases represent effective measurements performed on $\mathcal{H}_{\text{in}} \otimes \mathcal{H}_{\text{out}}$. Using ML estimation, we have reconstructed χ from the experimental data for 9 different values of ϕ. As an illustration, Fig. 3 depicts the reconstructed $\sqrt{\text{SWAP}}$ gate ($\phi = \pi/2$). In order to quantify the quality of the operation we use process fidelity defined as $F_\chi = \text{Tr}[\chi\chi_{\text{id}}]/(\text{Tr}[\chi]\text{Tr}[\chi_{\text{id}}])$. Here χ_{id} represents the ideal unitary transformation (1), which means that χ_{id} is effectively a pure state. The fidelities are given in Table I. Again, we can see that the lowest fidelity is exhibited by the $\sqrt{\text{SWAP}}$ gates, $F_\chi = 0.906$ for $\phi = \pi/2$ and $F_\chi = 0.888$ for $\phi = 3\pi/2$. The identity and SWAP operations achieve the highest fidelities, exceeding 0.94. These figures compare favorably with the values of the process fidelity of the linear-optical CNOT and CPHASE gate reported in previous experiments [8–10]. The unique feature of our scheme is that it can reliably implement a whole class of inequivalent operations (1) simply by changing the length of one interferometer arm with a piezodriven translation.

A crucial property of the entangling two-qubit gates is their ability to generate entangled states from product inputs. Consider the input product state $|\Psi_{\text{in}}\rangle = |\psi\rangle \times (\alpha|\psi\rangle + \beta|\psi_\perp\rangle)$, where $|\psi\rangle$ is an arbitrary state and $\langle\psi|\psi_\perp\rangle = 0$. The output state $|\Psi_{\text{out}}\rangle = U_\phi|\Psi_{\text{in}}\rangle$ reads

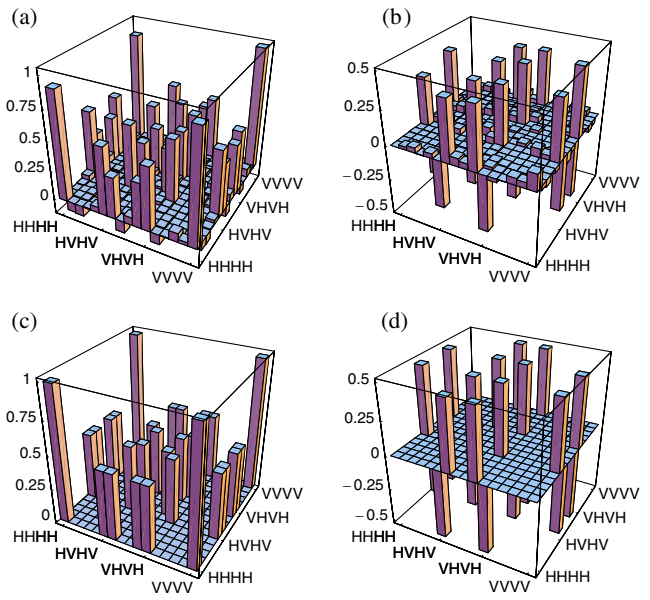

FIG. 3 (color online). $\sqrt{\text{SWAP}}$ gate ($\phi = \pi/2$). Real (a) and imaginary (b) parts of the reconstructed CP map χ are shown. Also the real (c) and imaginary (d) parts of the corresponding ideal map χ_{id} are plotted for comparison.

$$|\Psi_{\text{out}}\rangle = \alpha|\psi\psi\rangle + \beta e^{i\phi/2}\left(\cos\frac{\phi}{2}|\psi\psi_\perp\rangle - i\sin\frac{\phi}{2}|\psi_\perp\psi\rangle\right).$$

Its entanglement of formation is equal to the von Neumann entropy of the reduced density matrix of one of the qubits [1], $E_f = -x\log_2(x) - (1-x)\log_2(1-x)$, where $x = (1+\sqrt{1-|\beta|^4\sin^2\phi})/2$. In Fig. 4 we plot the entanglement of formation of the output state for four different input states $|D\rangle|D\rangle$, $|A\rangle|D\rangle$, $|H\rangle|D\rangle$ and $|R\rangle|D\rangle$. We observe good qualitative agreement with the theoretical expectations. The maximum entanglement $E_f = 0.815$ is obtained for input state $|A\rangle|D\rangle$ and $\phi = \pi/2$ which should ideally yield maximally entangled state. The state $|D\rangle|D\rangle$ is unaffected by U_ϕ so no entanglement is generated. Finally, the inputs $|H\rangle|D\rangle$ and $|R\rangle|D\rangle$ involve two nonorthogonal states, $|\beta|^2 = 1/2$ and only partially entangled states are produced.

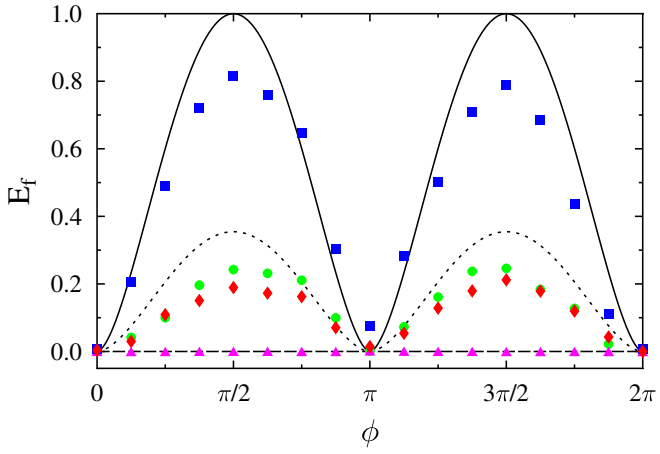

FIG. 4 (color online). Dependence of the entanglement of formation E_f of the output states on ϕ is plotted for four different input states $|D\rangle|D\rangle$ (▲), $|A\rangle|D\rangle$ (■), $|H\rangle|D\rangle$ (●) and $|R\rangle|D\rangle$ (◆). The lines show theoretical predictions. The measurements were performed for $\phi = k\pi/8$, $k = 0, \ldots, 16$.

In summary, we have proposed and demonstrated linear-optical partial SWAP gate for photonic qubits. The device operates with high fidelity and is easily tunable. Moreover, the setup can be easily converted into a filter performing partial symmetrization of polarization state of two photons by inserting an attenuator into one interferometer arm. This versatile scheme thus provides a valuable addition to the toolbox of available quantum linear-optics devices.

We thank Nicolas J. Cerf for many stimulating discussions and V. Michálek for technical assistance. This research was supported by the Projects No. LC06007, No. 1M06002, and No. MSM6198959213 of MSMT.

[1] M. A. Nielsen and I. L. Chuang, *Quantum Computation and Quantum Information* (Cambridge University Press, Cambridge, 2000).
[2] F. Schmidt-Kaler *et al.*, Nature (London) **422**, 408 (2003); D. Leibfried *et al.*, *ibid.* **422**, 412 (2003).
[3] A. M. Childs, I. L. Chuang, and D. W. Leung, Phys. Rev. A **64**, 012314 (2001).
[4] T. B. Pittman *et al.*, Phys. Rev. A **68**, 032316 (2003).
[5] J. L. O'Brien *et al.*, Nature (London) **426**, 264 (2003).
[6] S. Gasparoni *et al.*, Phys. Rev. Lett. **93**, 020504 (2004).
[7] Z. Zhao *et al.*, Phys. Rev. Lett. **94**, 030501 (2005).
[8] N. K. Langford *et al.*, Phys. Rev. Lett. **95**, 210504 (2005).
[9] N. Kiesel *et al.*, Phys. Rev. Lett. **95**, 210505 (2005).
[10] R. Okamoto *et al.*, Phys. Rev. Lett. **95**, 210506 (2005).
[11] X.-H. Bao *et al.*, Phys. Rev. Lett. **98**, 170502 (2007).
[12] J. Chen *et al.*, arXiv:0802.1441.
[13] E. Knill, R. Laflamme, and G. J. Milburn, Nature (London) **409**, 46 (2001).
[14] T. B. Pittman, B. C. Jacobs, and J. D. Franson, Phys. Rev. A **64**, 062311 (2001).
[15] T. C. Ralph *et al.*, Phys. Rev. A **65**, 012314 (2001).
[16] T. C. Ralph *et al.*, Phys. Rev. A **65**, 062324 (2002).
[17] P. Kok *et al.*, Rev. Mod. Phys. **79**, 135 (2007).
[18] Q. Zhang *et al.*, Nature Phys. **2**, 678 (2006).
[19] J. Fiurášek, Phys. Rev. A **73**, 062313 (2006).
[20] V. Scarani *et al.*, Phys. Rev. Lett. **88**, 097905 (2002).
[21] J. Fiurášek and N. J. Cerf, arXiv:0711.4212.
[22] J. Zhang, J. Vala, S. Sastry, and K. B. Whaley, Phys. Rev. A **69**, 042309 (2004).
[23] C. K. Hong, Z. Y. Ou, and L. Mandel, Phys. Rev. Lett. **59**, 2044 (1987).
[24] J. Soubusta *et al.*, Phys. Rev. A **76**, 042318 (2007).
[25] M. Ježek, J. Fiurášek, and Z. Hradil, Phys. Rev. A **68**, 012305 (2003).
[26] *Quantum State Estimation*, edited by M. G. A. Paris and J. Rehacek, Lect. Notes Phys. Vol. 649 (Springer, Berlin, 2004).